Int. J. Solids Structures Vol. 28, No. 1, pp. 43–65, 1991
Printed in Great Britain.

0020-7683/91 $3.00 + .00

MATRIX FRACTURE IN BRITTLE MATRIX FIBER-REINFORCED COMPOSITES

ANIL C. WIJEYEWICKREMA and LEON M. KEER
Department of Civil Engineering, Northwestern University, 2145 Sheridan Road, Evanston, IL 60208, U.S.A.

(*Received* 10 *March* 1990; *in revised form* 20 *August* 1990)

Abstract—A linear elastic fracture mechanics analysis of matrix cracking in a brittle matrix uniaxially fiber-reinforced composite due to uniform longitudinal strain is presented. The concentric circular cylinders model is used while perfect bonding is assumed at the fiber matrix interface. The axisymmetric problem of an elastic fiber surrounded by the elastic matrix containing an annular crack is formulated in terms of a singular integral equation of the first kind with a Cauchy-type kernel. Four possible crack configurations are considered as follows: (a) internal annular crack with inner crack tip away from the interface; (b) internal annular crack with inner crack tip at the interface; (c) annular edge crack with inner crack tip away from the interface; (d) annular edge crack with inner crack tip at the interface (fully cracked matrix). Stress intensity factors are given for a wide range of crack sizes for different ratios of shear moduli. Stress fields are presented for a typical brittle matrix fiber-reinforced composite, SiC/CAS calcium aluminosilicate glass ceramic reinforced with silicon carbide fibers.

INTRODUCTION

The mechanics of brittle matrix fracture in uniaxially fiber-reinforced composites loaded by uniform longitudinal tensile strain is considered in the present analysis when the fibers are perfectly bonded to the matrix. The high-strength fibers which reinforce the brittle matrix have in most instances a fracture strain much higher than that of the matrix and the first matrix cracks appear in a plane perpendicular to the direction of loading. This phenomenon has been observed in experiments carried out on different materials. In particular, Prewo and Brennan (1982), Marshall and Evans (1985) and Daniel *et al.* (1989) have conducted experiments on glass ceramics reinforced by SiC fibers.

The initial theoretical works on this important problem of brittle matrix fracture were by Aveston *et al.* (1971) and by Aveston and Kelly (1973), where various assumptions were made to facilitate the analysis. Subsequent work in this area is due to Marshall *et al.* (1985), Budiansky *et al.* (1986), McCartney (1987, 1989), Gao *et al.* (1988) and Sigl and Evans (1989). An approximate analytic method was employed by McCartney (1989) to investigate matrix cracking with perfect bonding between the fibers and the matrix and also with fractional slip at the interface. Recently, Wijeyewickrema *et al.* (1991) considered the case of matrix cracking when a single elastic fiber is perfectly bonded to a surrounding unbounded elastic matrix.

The chief objective of this paper is to present a rigorous analysis of the problem of brittle matrix fracture when there is perfect bonding at the interface, within the context of linear elastic fracture mechanics (LEFM) where the correct nature of the singular stress fields is preserved.

The problem of a thick-walled elastic cylinder with an annular crack considered by Erdol and Erdogan (1978) and by Nied and Erdogan (1983) corresponds to the case where the fibers are replaced by cavities. The solid elastic cylinder with an edge crack investigated by Keer *et al.* (1977) corresponds to an elastic fiber with the same material properties as the matrix.

FORMULATION OF PROBLEM

It is well known through experimental observations that in general the fibers in a uniaxial fiber-reinforced composite are not distributed in any particular order. In theoretical

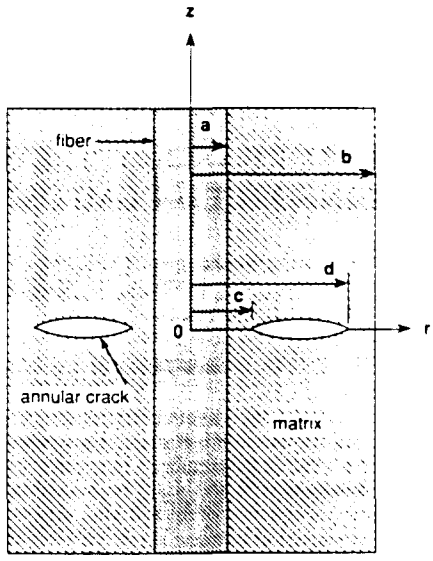

Fig. 1. An annular matrix crack surrounding the elastic fiber. Approximation to the case of a hexagonal array of fibers in a matrix where the concentric circular cylinders model represents a unit cell.

considerations, to overcome this lack of orderly distribution of fibers, an orderly distribution of fibers such as a square or hexagonal array is assumed (Jones, 1975). When a hexagonal array of fibers is assumed, due to considerations of symmetry it is sufficient to consider the unit cell of a fiber surrounded by a tube of matrix which has a hexagonal cylinder for the outer surface. When this hexagonal cylindrical surface is approximated by a circular cylindrical surface of equal cross-sectional area so as to make the geometry of the problem analytically less complex, the concentric circular cylinders model results. This axisymmetric model has been used by many researchers investigating the mechanical behavior of composites under longitudinal loading (Hill, 1964a,b; Smith and Spencer, 1970; Steif, 1984; Budiansky *et al.*, 1986; Gao *et al.*, 1988; McCartney, 1989; Sigl and Evans, 1989).

The concentric cylinders model and the cylindrical polar coordinate system (r, θ, z) used in this analysis is shown in Fig. 1, where an infinitely-long elastic fiber of radius a is perfectly bonded to the elastic matrix which has an outer radius b. When a uniaxial fiber-reinforced composite which has a fiber volume ratio of V_f is considered, $b = a/V_f^{1/2}$. Matrix cracks appear at a uniform longitudinal tensile strain ε_0 applied to the system at $z = \pm \infty$. The crack plane which is normal to the z axis is taken as the $z = 0$ plane. The inner and outer radii of the annular crack are c and d, respectively $(a \leqslant c < b, a < d \leqslant b)$.

When the undamaged composite specimen is loaded longitudinally, there is radial contraction due to the Poisson's ratio effect. Prior to the formation of matrix cracks, the external surface of the entire lateral surface of the specimen, and hence of each concentric circular cylindrical cell, will be stress free. When the applied strain reaches the matrix fracture strain, matrix cracks appear and the external surface of the circular cylindrical cell may not be stress free, since the matrix cracks will produce radial stresses that arise at the outer boundary. This situation can be physically visualized as the superposition of two problems: the undamaged uniaxially-loaded composite specimen and a matrix cracked specimen loaded solely on the cracked surface. The undamaged specimen problem has the outer boundary stress free; however, the matrix crack problem will have a zero radial displacement at the outer boundary. The superposition of these two problems will correctly model the case of interest here.

In the first problem the concentric cylinder model in the absence of the annular crack is subjected to the uniform longitudinal tensile strain ε_0, while the external surface is unconstrained. This problem can be solved with ease and the complete stress field is given in Appendix A. The relevant matrix stresses required for the second problem are $\sigma_{zz}^1(r)$ and $\sigma_{rz}^1(r)$ given by eqns (A7) and (A8), respectively. Since $\sigma_{rz}^1(r, 0)$ is identically equal to zero,

the self-equilibrating stresses applied to the crack surfaces in the second problem are those equal and opposite to the stresses $\sigma_{zz}^{1}(r,0)$.

The analytical approach and the notation adopted in solving the problem where the crack surface tractions are the only external loads, is for the most part similar to that employed previously by Wijeyewickrema *et al.* (1991) to solve the problem of an annular crack surrounding a single elastic fiber embedded in an elastic full space. For problems where both the geometry of the problem and the loading is axially symmetric the nonvanishing displacement and stress components u_r, u_z, σ_{rr}, $\sigma_{\theta\theta}$, σ_{zz} and σ_{rz} can be expressed in terms of Love's stress function $\chi(r,z)$, which is an axisymmetric biharmonic function (Love, 1944, p. 276; Timoshenko and Goodier, 1970, p. 381). Since $z = 0$ is a plane of symmetry, in what follows the upper half of the representative cell $z \geqslant 0$ is considered.

For the fiber, Love's stress function and the corresponding displacements and stresses which are relevant are given by

$$\chi^{0}(r,z) = \frac{2}{\pi}\int_0^{\infty}[f_1(s)I_0(rs)+f_2(s)rsI_1(rs)]\sin(zs)\,ds + \int_0^{\infty} f_3(p)p(2\nu_0+zp)\,e^{-zp}J_0(rp)\,dp, \tag{1}$$

$$u_r^{0}(r,z) = -\frac{1}{2\mu_0}\left\{\frac{2}{\pi}\int_0^{\infty}[f_1(s)I_1(rs)+f_2(s)rsI_0(rs)]s^2\cos(zs)\,ds - \int_0^{\infty} f_3(p)p^3(1-2\nu_0-zp)\,e^{-zp}J_1(rp)\,dp\right\}, \tag{2}$$

$$u_z^{0}(r,z) = \frac{1}{2\mu_0}\left\{\frac{2}{\pi}\int_0^{\infty}[f_1(s)I_0(rs)+f_2(s)[4(1-\nu_0)I_0(rs)+rsI_1(rs)]]s^2\sin(zs)\,ds - \int_0^{\infty} f_3(p)p^3[2(1-\nu_0)+zp]\,e^{-zp}J_0(rp)\,dp\right\}, \tag{3}$$

$$\sigma_{rr}^{0}(r,z) = \frac{2}{\pi}\int_0^{\infty}\{f_1(s)[-I_0(rs)+I_1(rs)/rs]+f_2(s)[(2\nu_0-1)I_0(rs)-rsI_1(rs)]\}s^3\cos(zs)\,ds + \int_0^{\infty} f_3(p)p^4[(1-zp)J_0(rp)-(1-2\nu_0-zp)J_1(rp)\,rp]\,e^{-zp}\,dp, \tag{4}$$

$$\sigma_{zz}^{0}(r,z) = \frac{2}{\pi}\int_0^{\infty}\{f_1(s)I_0(rs)+f_2(s)[2(2-\nu_0)I_0(rs)+rsI_1(rs)]\}s^3\cos(zs)\,ds + \int_0^{\infty} f_3(p)p^4(1+zp)\,e^{-zp}J_0(rp)\,dp, \tag{5}$$

$$\sigma_{rz}^{0}(r,z) = \frac{2}{\pi}\int_0^{\infty}\{f_1(s)I_1(rs)+f_2(s)[rsI_0(rs)+2(1-\nu_0)I_1(rs)]\}s^3\sin(zs)\,ds + \int_0^{\infty} f_3(p)p^5z\,e^{-zp}J_1(rp)\,dp, \tag{6}$$

where $f_i(s)$, $(i = 1, 2, 3)$ are unknown functions, $J_n(\ )$ is the Bessel function of the first kind of order n, $I_n(\ )$ is the modified Bessel function of the first kind of order n and μ_0 and ν_0 are the fiber shear modulus and Poisson's ratio, respectively.

For the matrix region, Love's stress function and the corresponding displacements and stresses that are relevant are given by

$$\chi^1(r,z) = \frac{2}{\pi}\int_0^\infty [f_4(s)I_0(rs)+f_5(s)rsI_1(rs)+f_6(s)K_0(rs)+f_7(s)rsK_1(rs)]\sin(zs)\,ds + \int_0^\infty f_8(p)p(2\nu_1+zp)\,e^{-zp}J_0(rp)\,dp, \quad (7)$$

$$u_r^1(r,z) = -\frac{1}{2\mu_1}\left\{\frac{2}{\pi}\int_0^\infty [f_4(s)I_1(rs)+f_5(s)rsI_0(rs)-f_6(s)K_1(rs)-f_7(s)rsK_0(rs)]s^2\cos(zs)\,ds - \int_0^\infty f_8(p)p^2(1-2\nu_1-zp)\,e^{-zp}J_1(rp)\,dp\right\}, \quad (8)$$

$$u_z^1(r,z) = \frac{1}{2\mu_1}\left\{\frac{2}{\pi}\int_0^\infty [f_4(s)I_0(rs)+f_5(s)[4(1-\nu_1)I_0(rs)+rsI_1(rs)]+f_6(s)K_0(rs) + f_7(s)[-4(1-\nu_1)K_0(rs)+rsK_1(rs)]]s^2\sin(zs)\,ds - \int_0^\infty f_8(p)p^2[2(1-\nu_1)+zp]\,e^{-zp}J_0(rp)\,dp\right\}, \quad (9)$$

$$\sigma_{rr}^1(r,z) = \frac{2}{\pi}\int_0^\infty \{f_4(s)[-I_0(rs)+I_1(rs)/rs]-f_5(s)[(1-2\nu_1)I_0(rs)+rsI_1(rs)] - f_6(s)[K_0(rs)+K_1(rs)/rs]+f_7(s)[(1-2\nu_1)K_0(rs)-rsK_1(rs)]\}s^3\cos(zs)\,ds + \int_0^\infty f_8(p)p^4[(1-zp)J_0(rp)-(1-2\nu_1-zp)J_1(rp)/rp]\,e^{-zp}\,dp, \quad (10)$$

$$\sigma_{zz}^1(r,z) = \frac{2}{\pi}\int_0^\infty \{f_4(s)I_0(rs)+f_5(s)[2(2-\nu_1)I_0(rs)+rsI_1(rs)] + f_6(s)K_0(rs)+f_7(s)[-2(2-\nu_1)K_0(rs)+rsK_1(rs)]\}s^3\cos(zs)\,ds + \int_0^\infty f_8(p)p^4(1+zp)\,e^{-zp}J_0(rp)\,dp, \quad (11)$$

$$\sigma_{rz}^1(r,z) = \frac{2}{\pi}\int_0^\infty \{f_4(s)I_1(rs)+f_5(s)[rsI_0(rs)+2(1-\nu_1)I_1(rs)]-f_6(s)K_1(rs) + f_7(s)[-rsK_0(rs)+2(1-\nu_1)K_1(rs)]\}s^3\sin(zs)\,ds + \int_0^\infty f_8(p)p^5z\,e^{-zp}J_1(rp)\,dp \quad (12)$$

where the functions $f_i(s)$, $(i = 4, \ldots, 8)$ are to be determined and $K_n(\ )$ is the modified Bessel function of the second kind of order n where μ_1 and ν_1 are the matrix shear modulus and Poisson's ratio, respectively.

The perfect fiber-matrix bonding assumed at the interface results in the continuity conditions

$$u_r^0(a,z) = u_r^1(a,z), \quad u_z^0(a,z) = u_z^1(a,z), \quad 0 \leqslant z < \infty, \quad (13)$$

$$\sigma_{rr}^0(a,z) = \sigma_{rr}^1(a,z), \quad \sigma_{rz}^0(a,z) = \sigma_{rz}^1(a,z), \quad 0 \leqslant z < \infty. \quad (14)$$

As discussed previously, the boundary conditions on the external cylindrical surface of the matrix are taken as

$$u_r^1(b,z) = 0, \quad 0 \leqslant z < \infty, \tag{15}$$

$$\sigma_{rz}^1(b,z) = 0, \quad 0 \leqslant z < \infty. \tag{16}$$

On the plane $z = 0$, the following conditions apply

$$\sigma_{rz}^0(r,0) = 0, \quad 0 \leqslant r \leqslant a, \quad \sigma_{rz}^1(r,0) = 0, \quad a \leqslant r \leqslant b, \tag{17}$$

$$\sigma_{zz}^1(r,0) = -p(r), \quad c < r < d, \tag{18}$$

$$u_z^0(r,0) = 0, \quad 0 \leqslant r \leqslant a, \quad u_z^1(r,0) = 0, \quad a \leqslant r < c, \quad d < r \leqslant b. \tag{19}$$

It is easily verified from eqns (6) and (12) that eqn (17) is identically satisfied. From the first part of eqn (19) and eqn (3) it can be shown that $f_3(p) = 0$. To formulate the problem in terms of an integral equation a new unknown function $\phi(r)$ which is related to the gradient of the crack opening displacement is introduced as follows

$$\frac{\mu_1}{1-\nu_1}\frac{\partial}{\partial r}u_z^1(r,0) = \phi(r), \quad c < r < d. \tag{20}$$

It can be shown from eqns (9), (20) and the second part of eqn (19) that

$$p^{\frac{1}{2}}f_8(p) = \int_c^d t\phi(t)J_1(pt)\,\mathrm{d}t. \tag{21}$$

The four boundary conditions at the interface eqns (13) and (14) and the boundary conditions on the external surface of the matrix eqns (15) and (16) yield a system of six equations for the unknown functions f_i, $(i = 1, 2, 4, 5, 6, 7)$ in terms of the unknown function $\phi(r)$ and may be expressed as follows

$$I_1(as)f_1(s) + asI_0(as)f_2(s) - \tilde{\mu}I_1(as)f_4(s) - \tilde{\mu}asI_0(as)f_5(s) + \tilde{\mu}K_1(as)f_6(s) + \tilde{\mu}asK_0(as)f_7(s) = \frac{1}{s^3}\int_c^d t\phi(t)h_1(t,s)\,\mathrm{d}t, \tag{22}$$

$$I_0(as)f_1(s) + [4(1-\nu_0)I_0(as) + asI_1(as)]f_2(s) - \tilde{\mu}I_0(as)f_4(s) - \tilde{\mu}[4(1-\nu_1)I_0(as) + asI_1(as)]f_5(s) - \tilde{\mu}K_0(as)f_6(s) + \tilde{\mu}[4(1-\nu_1)K_0(as) - asK_1(as)]f_7(s) = \frac{1}{s^3}\int_c^d t\phi(t)h_2(t,s)\,\mathrm{d}t, \tag{23}$$

$$[-I_0(as) + I_1(as)/as]f_1(s) - [(1-2\nu_0)I_0(as) + asI_1(as)]f_2(s) + [I_0(as) - I_1(as)/as]f_4(s) + [(1-2\nu_1)I_0(as) + asI_1(as)]f_5(s) + [K_0(as) + K_1(as)/as]f_6(s) + [-(1-2\nu_1)K_0(as) + asK_1(as)]f_7(s) = \frac{1}{s^3}\int_c^d t\phi(t)h_3(t,s)\,\mathrm{d}t, \tag{24}$$

$$I_1(as)f_1(s)+[asI_0(as)+2(1-\nu_0)I_1(as)]f_2(s)-I_1(as)f_4(s)$$
$$-[asI_0(as)+2(1-\nu_1)I_1(as)]f_5(s)+K_1(as)f_6(s)+[asK_0(as)-2(1-\nu_1)K_1(as)]f_7(s)$$
$$=\frac{1}{s^3}\int_c^d t\phi(t)h_4(t,s)\,dt, \quad (25)$$

$$I_1(bs)f_4(s)+bsI_0(bs)f_5(s)-K_1(bs)f_6(s)-bsK_0(bs)f_7(s)=\frac{1}{s^3}\int_c^d t\phi(t)h_5(t,s)\,dt, \quad (26)$$

$$I_1(bs)f_4(s)+[bsI_0(bs)+2(1-\nu_1)I_1(bs)]f_5(s)-K_1(bs)f_6(s)$$
$$+[-bsK_0(bs)+2(1-\nu_1)K_1(bs)]f_7(s)=\frac{1}{s^3}\int_c^d t\phi(t)h_6(t,s)\,dt, \quad (27)$$

where $\bar{\mu}=\mu_0/\mu_1$ and the functions h_i, $(i=1,\ldots,6)$ are given by

$$h_1(t,s)=\bar{\mu}s\{asI_0(as)K_1(ts)-tsI_1(as)K_0(ts)-2(1-\nu_1)I_1(as)K_1(ts)\}, \quad (28)$$

$$h_2(t,s)=\bar{\mu}s\{-tsI_0(as)K_0(ts)+2(1-\nu_1)I_0(as)K_1(ts)+asI_1(as)K_1(ts)\}, \quad (29)$$

$$h_3(t,s)=s\left\{tsI_0(as)K_0(ts)+I_0(as)K_1(ts)-\frac{t}{a}I_1(as)K_0(ts)-\left[as+\frac{2(1-\nu_1)}{as}\right]I_1(as)K_1(ts)\right\}, \quad (30)$$

$$h_4(t,s)=s\{asI_0(as)K_1(ts)-tsI_1(as)K_0(ts)\}, \quad (31)$$

$$h_5(t,s)=s\{-tsI_0(ts)K_1(bs)+bsI_1(ts)K_0(bs)+2(1-\nu_1)I_1(ts)K_1(bs)\}, \quad (32)$$

$$h_6(t,s)=s\{-tsI_0(ts)K_1(bs)+bsI_1(ts)K_0(bs)\}. \quad (33)$$

Infinite integrals required in deriving eqns (22) to (27) can be found in Erdelyi (1954). Solving the system of six equations given by eqns (22)–(27), f_i, $(i=1, 2, 4\text{–}7)$ can be expressed as

$$f_i(s)=\int_c^d t\phi(t)\,dt\,\frac{1}{s^3}\sum_{j=1}^{6}\frac{A_{ij}(s)h_j(t,s)}{\Delta(s)}, \quad (34)$$

where $\Delta(s)$ is the determinant and A_{ij}, $(i=1, 2, 4\text{–}7; j=1\text{–}6)$ are the appropriate elements of the adjoint of the coefficient matrix of eqns (22)–(27). From eqn (18), which corresponds to the tractions that are applied to the crack surface, after substituting for f_i, $(i=4\text{–}8)$ from eqns (34) and (21), the following integral equation is obtained:

$$\frac{1}{\pi}\int_c^d\left[\frac{1}{t-r}+k(r,t)\right]\phi(t)\,dt=-p(r), \quad c<r<d \quad (35)$$

where

$$k(r,t)=k_1(r,t)+2tk_2(r,t), \quad (36)$$

$$k_1(r,t)=\frac{m(r,t)-1}{t-r}+\frac{m(r,t)}{t+r}, \quad (37)$$

$$m(r,t)=\begin{cases} E(r/t) & r<t \\ \dfrac{r}{t}E(t/r)+\dfrac{(t^2-r^2)}{rt}K(t/r), & r>t \end{cases} \tag{38}$$

$$k_2(r,t)=\int_0^\infty \bar{k}_2(r,t,s)\,\mathrm{d}s, \tag{39}$$

$$\bar{k}_2(r,t,s)=\frac{1}{\Delta(s)}\left\{\left(\sum_{i=1}^{6}A_{4i}h_i\right)I_0(rs)+\left(\sum_{i=1}^{6}A_{5i}h_i\right)[2(2-\nu_1)I_0(rs)+rsI_1(rs)]\right.$$
$$\left.+\left(\sum_{i=1}^{6}A_{6i}h_i\right)K_0(rs)+\left(\sum_{i=1}^{6}A_{7i}h_i\right)[-2(2-\nu_1)K_0(rs)+rsK_1(rs)]\right\}, \tag{40}$$

where $K(\ )$ and $E(\ )$ are the complete elliptic integrals of the first and second kind, respectively. The location of the crack in the matrix has a direct bearing on the solution of the singular integral equation of the first kind, eqn (35). When both crack tips c and d are located in the matrix, eqn (35) is solved under the crack closure condition

$$\int_c^d \phi(r)\,\mathrm{d}r=0, \tag{41}$$

obtained from the second eqn of (19) and eqn (20). It is noted that the physical significance of eqn (41) is that the crack tips are closed at c and d.

The following crack configurations are investigated in detail in the present analysis:

Case I: Internal annular crack with inner crack tip away from the interface.
Case II: Internal annular crack with inner crack tip at the interface.
Case III: Annular edge crack with inner crack tip away from the interface.
Case IV: Annular edge crack with inner crack tip at the interface (fully cracked matrix).

CASE I: INTERNAL ANNULAR CRACK WITH INNER CRACK TIP AWAY FROM THE INTERFACE

When the crack tips are located such that $a<c<d<b$, the dominant kernel in the integral eqn (35) is the term $1/(t-r)$. The kernel $k_1(r,t)$ has a logarithmic singularity of the form $\log|t-r|$ and $k_2(r,t)$ is bounded in the interval $c\leqslant r,\ t\leqslant d$. The solution of eqn (35) is of the form

$$\phi(t)=(d-t)^{-1/2}(t-c)^{-1/2}g_1(t), \quad c<t<d \tag{42}$$

where $g_1(t)$ is a bounded function. Normalizing the interval (c,d) by defining

$$t=\frac{d-c}{2}\tau+\frac{d+c}{2}, \quad r=\frac{d-c}{2}\rho+\frac{d+c}{2}, \tag{43}$$

$$\phi(t)=h_1(\tau)=(1-\tau^2)^{-1/2}F_1(\tau), \tag{44}$$

$$p(r)=P(\rho), \quad K(\rho,\tau)=\frac{d-c}{2}k(r,t), \tag{45}$$

the following equations are obtained.

$$\frac{1}{\pi}\int_{-1}^{1}\left[\frac{1}{\tau-\rho}+K(\rho,\tau)\right]\frac{F_1(\tau)}{(1-\tau^2)^{1/2}}\,d\tau=-P(\rho),\quad -1<\rho<1 \tag{46}$$

$$\int_{-1}^{1}\frac{F_1(\tau)}{(1-\tau^2)^{1/2}}\,d\tau=0. \tag{47}$$

Here eqn (47) corresponds to the crack closure condition eqn (41) since the crack tips are closed at c and d. The singular integral eqn (46) is solved together with the additional condition eqn (47) by using a Gauss–Chebyshev type quadrature formula (Erdogan and Gupta, 1972).

The mode I stress intensity factors at the crack tips c and d are defined by

$$K(c)=\lim_{r\to c}\sqrt{2(c-r)}\sigma_{zz}^{1}(r,0), \tag{48}$$

$$K(d)=\lim_{r\to d}\sqrt{2(r-d)}\sigma_{zz}^{1}(r,0), \tag{49}$$

and can be expressed in terms of $F_1(\tau)$ as follows

$$K(c)=\lim_{r\to c}\sqrt{2(r-c)}\phi(r)=a_1^{1/2}F_1(-1), \tag{50}$$

$$K(d)=-\lim_{r\to d}\sqrt{2(d-r)}\phi(r)=-a_1^{1/2}F_1(1), \tag{51}$$

where $a_1=(d-c)/2$. The compact formulae given by Krenk (1975) is used to obtain $F_1(-1)$ and $F_1(1)$.

CASE II: INTERNAL ANNULAR CRACK WITH INNER CRACK TIP AT THE INTERFACE

When the inner crack tip is at the interface, i.e. $c=a$, $k_2(r,t)$ given by eqn (39) is no longer bounded for all r,t in the closed interval $[c,d]$ and hence the solution of eqn (35) is no longer described by eqn (42). By adding and subtracting the asymptotic value of $\bar{K}_2(r,t,s)$ for large values of s, from the integrand in eqn (39), $k_2(r,t)$ may be expressed as

$$k_2(r,t)=k_{2f}(r,t)+k_{2s}(r,t), \tag{52}$$

where

$$k_{2f}(r,t)=\int_0^{\infty}[\bar{K}_2(r,t,s)-\bar{K}_2^{a,r}(r,t,s)]\,ds+I_{2f}^{a,r}(r,t), \tag{53}$$

$$\bar{K}_2^{a,r}(r,t,s)=[R_{11}s^2+R_{12}s+R_{13}]\frac{e^{-(r+t-2a)s}}{2\sqrt{rt}}, \tag{54}$$

$$I_{2f}^{a,r}(r,t)=\frac{1}{2\sqrt{rt}}\left[\sum_{i=1}^{6}S_{1i}+\sum_{i=1}^{3}T_{1i}\right], \tag{55}$$

$$k_{2s}(r,t)=I_{2s}^{a,r}(r,t), \tag{56}$$

$$I_{2s}^{a,r}(r,t)=\frac{1}{2\sqrt{rt}}\left\{\frac{c_0}{(r+t-2a)}-\frac{c_1(r-a)}{(r+t-2a)^2}+\frac{2c_2(r-a)^2}{(r+t-2a)^3}\right\}, \tag{57}$$

$$c_0 = \frac{1}{2}\left[1 - \frac{\bar{\mu}(1+\kappa_1)}{\bar{\mu}+\kappa_0} - \frac{3(1-\bar{\mu})}{1+\bar{\mu}\kappa_1}\right], \quad c_1 = -\frac{6(1-\bar{\mu})}{1+\bar{\mu}\kappa_1}, \quad c_2 = -\frac{2(1-\bar{\mu})}{1+\bar{\mu}\kappa_1}, \tag{58}$$

where R_{ij}, T_{ij}, $(i = 1, 2, 3)$ and S_{ij}, $(i = 1, \ldots, 6)$ are given in Appendix B and $\kappa_i = 3-4\nu_i$, $(i = 0, 1)$. In eqn (53), $k_2(r, t)$ is bounded in $[c, d]$ for all r, t and $k_3(r, t)$ is unbounded as r and t approach a. The singular kernel $k_3(r, t)$ is identical to that given by Erdogan *et al.* (1973) for the corresponding plane strain problem and by Wijeyewickrema *et al.* (1991) for the case of an annular crack surrounding an elastic fiber embedded in an elastic full space.

Equation (35) can now be rewritten as

$$\frac{1}{\pi}\int_a^d \frac{\phi(t)}{t-r}\,dt + \frac{1}{\pi}\int_a^d l_1(r, t)\phi(t)\,dt + \frac{1}{\pi}\int_a^d l_2(r, t)\phi(t)\,dt = -p(r), \quad a < r < d \tag{59}$$

where

$$l_1(r, t) = 2tk_3(r, t), \tag{60}$$

$$l_2(r, t) = k_1(r, t) + 2tk_2(r, t), \tag{61}$$

and where $l_2(r, t)$ is a Fredholm kernel.

The solution of eqn (59) is expressed as

$$\phi(t) = (d-t)^{\alpha}(t-a)^{\beta}g_2(t), \quad a < t < d \tag{62}$$

and it can be shown (Erdogan *et al.*, 1973) that the characteristic equations required to determine α and β are given by

$$\cot \pi\alpha = 0, \tag{63}$$

$$2d_1 \cos \pi(\beta+1) - d_2(\beta+1)^2 - d_3 = 0, \tag{64}$$

where

$$d_1 = (\bar{\mu}+\kappa_0)(1+\bar{\mu}\kappa_1), \tag{65}$$

$$d_2 = -4(1-\bar{\mu})(\bar{\mu}+\kappa_0), \tag{66}$$

$$d_3 = (1-\bar{\mu})(\bar{\mu}+\kappa_0) + (\bar{\mu}+\kappa_0)(1+\bar{\mu}\kappa_1) - \bar{\mu}(1+\kappa_1)(1+\bar{\mu}\kappa_1). \tag{67}$$

From eqn (63), $\alpha = -\frac{1}{2}$ which is the expected square root singularity for the crack tip d. Equation (64) is solved to determine the real constant β which is a function of the material properties of the fiber and matrix.

Normalizing the interval (a, d) by defining

$$t = \frac{d-a}{2}\tau + \frac{d+a}{2}, \quad r = \frac{d-a}{2}\rho + \frac{d+a}{2}, \tag{68}$$

$$\phi(t) = h_2(\tau) = (1-\tau)^{\alpha}(\tau+1)^{\beta}F_2(\tau), \tag{69}$$

$$L_1(\rho, \tau) = \frac{d-a}{2}l_1(r, t), \quad L_2(\rho, \tau) = \frac{d-a}{2}l_2(r, t), \tag{70}$$

$$p(r) = P(\rho), \tag{71}$$

eqn (59) can be expressed as

$$\frac{1}{\pi}\int_{-1}^{1}\left\{\frac{1}{\tau-\rho}+L_1(\rho,\tau)+L_2(\rho,\tau)\right\}F_2(\tau)(1-\tau)^{\alpha}(\tau+1)^{\beta}\,d\tau=-P(\rho),\quad -1<\rho<1. \tag{72}$$

Since the crack tips are closed at a and d, the crack closure condition (41) yields the equation

$$\int_{-1}^{1}F_2(\tau)(1-\tau)^{\alpha}(\tau+1)^{\beta}\,d\tau=0. \tag{73}$$

A Gauss–Jacobi-type integration formula (Erdogan *et al.*, 1973) is used to solve the singular integral equation with a generalized Cauchy kernel, eqn (72), together with the crack closure condition, eqn (73).

The mode I stress intensity factors at the crack tips d and a are defined by

$$K(d)=\lim_{r\to d}\sqrt{2(r-d)}\sigma_{zz}^{1}(r,0), \tag{74}$$

$$K(a)=\lim_{r\to a}2^{1-\beta}(a-r)^{-\beta}\sigma_{zz}^{0}(r,0). \tag{75}$$

It can be shown that

$$K(d)=-2^{1-\beta}(d-a)^{\beta}g_2(d)=-\lim_{r\to d}2^{1-\beta}(d-r)^{-\beta}\phi(r)=-2^{\beta+1-\beta}a_2^{1-\beta}F_2(1), \tag{76}$$

$$K(a)=2^{1-\beta}\mu^{*}(c-a)^{\alpha}g_2(a)=\mu^{*}\lim_{r\to a}2^{1-\beta}(r-a)^{-\beta}\phi(r)=\mu^{*}a_2^{-\beta}F_2(-1), \tag{77}$$

where

$$\mu^{*}=\frac{\bar{\mu}(1+\kappa_1)}{2}\left\{\frac{(3+2\beta)(1+\bar{\mu}\kappa_1)-(1+2\beta)(\bar{\mu}+\kappa_0)}{(\bar{\mu}+\kappa_0)(1+\bar{\mu}\kappa_1)\sin\pi(1+\beta)}\right\} \tag{78}$$

and $a_2=(d-a)/2$. In calculating $F_2(-1)$ and $F_2(1)$ a formula given by Krenk (1975) is used.

CASE III: ANNULAR EDGE CRACK WITH INNER CRACK TIP AWAY FROM THE INTERFACE

For this crack configuration where $a<c<d$ and $d=b$ the kernel $k_2(r,t)$ defined by eqn (39) becomes unbounded for large values of s when r and t approach the boundary b. After manipulating $k_2(r,t)$ similar to the procedure adopted in Case II, $k_2(r,t)$ is expressed as

$$k_2(r,t)=k_{2f}(r,t)+k_{2s}(r,t); \tag{79}$$

here

$$k_{2f}(r,t)=\int_0^{\infty}[\bar{K}_2(r,t,s)-\bar{K}_2^{b,c}(r,t,s)]\,ds+I_{2f}^{b,c}(r,t), \tag{80}$$

$$\bar{K}_2^{b,c}(r,t,s)=[R_{22}s+R_{23}]\frac{e^{-(2b-r-t)s}}{2\sqrt{rt}}, \tag{81}$$

$$I_{2f}^{b,c}(r,t)=\frac{1}{2\sqrt{rt}}\sum_{i=1}^{2}S_{2i}, \tag{82}$$

$$k_{23}(r,t) = I_{23}^{bc}(r,t), \tag{83}$$

$$I_{23}^{bc}(r,t) = \frac{1}{2\sqrt{rt}}\left\{\frac{-1}{2b-r-t}\right\}, \tag{84}$$

where R_{2i}, $(i=2,3)$ and S_{2i}, $(i=1,2)$ are given in Appendix B. In eqn (80), $k_{2f}(r,t)$ is bounded in $[c,b]$ for all r, t and $k_{23}(r,t)$ is unbounded as r and t approach b. The solution of the integral equation which now has a generalized Cauchy kernel has no power or logarithmic singularity at the end point which is on the boundary $r=b$, and the solution is of the form

$$\phi(t) = (t-c)^{-1/2}g_3(t), \quad c<t<b. \tag{85}$$

From eqn (85) it is seen that $\phi(t)$ is bounded at $t=b$. Normalizing the interval (c,b) by defining

$$t = \frac{b-c}{2}\tau + \frac{b+c}{2}, \quad r = \frac{b-c}{2}\rho + \frac{b+c}{2}, \tag{86}$$

$$\phi(t) = h_3(\tau) = (1-\tau^2)^{-1/2}F_3(\tau), \tag{87}$$

$$p(r) = P(\rho), \quad K(\rho,\tau) = \frac{b-c}{2}k(r,t), \tag{88}$$

the integral equation is obtained as

$$\frac{1}{\pi}\int_{-1}^{1}\left[\frac{1}{\tau-\rho}+K(\rho,\tau)\right]\frac{F_3(\tau)}{(1-\tau^2)^{1/2}}\,d\tau = -P(\rho), \quad -1<\rho<1. \tag{89}$$

The function $F_3(\tau)$ is obtained by using a Gauss–Chebyshev-type quadrature formula (Erdogan and Gupta, 1972) and solving the singular integral eqn (89) numerically together with the additional condition $F_3(1)=0$, to account for the boundedness of $\phi(t)$ at $t=b$.

The mode I stress intensity factor at the crack tip c is defined by

$$K(c) = \lim_{r\to c}\sqrt{2(c-r)}\sigma_{zz}^{1}(r,0), \tag{90}$$

and can be expressed as

$$K(c) = \lim_{r\to c}\sqrt{2(r-c)}\phi(r) = a_3^{1/2}F_3(-1), \tag{91}$$

where $a_3=(b-c)/2$. Here too recourse is made to a formula given by Krenk (1975) to obtain $F_3(-1)$.

CASE IV: ANNULAR EDGE CRACK WITH INNER CRACK TIP AT THE INTERFACE (FULLY CRACKED MATRIX)

When $c=a$ and $d=b$, on the plane $z=0$, stress is transferred through the fibers only. The kernel $k_2(r,t)$ given by eqn (39) is now expressed as

$$k_2(r,t) = k_{2f}(r,t)+k_{23}(r,t), \tag{92}$$

where

$$k_{2j}(r,t)=\int_0^c [\bar{K}_2(r,t,s)-\bar{K}_2^{a,c}(r,t,s)-\bar{K}_2^{b,c}(r,t,s)]\,ds+I_{2j}^{a,c}(r,t)+I_{2j}^{b,c}(r,t), \tag{93}$$

$$k_{2s}(r,t)=I_{2s}^{a,c}(r,t)+I_{2s}^{b,c}(r,t). \tag{94}$$

The solution of the integral equation which now has a generalized Cauchy kernel is of the form

$$\phi(t)=(t-a)^{\beta}g_4(t), \quad a<t<b. \tag{95}$$

From eqn (95) it is seen that $\phi(t)$ is bounded at $t=b$. Normalizing the interval (a,b) by defining

$$t=\frac{b-a}{2}\tau+\frac{b+a}{2}, \quad r=\frac{b-a}{2}\rho+\frac{b+a}{2}, \tag{96}$$

$$\phi(t)=h_4(\tau)=(1-\tau)^{-1/2}(\tau+1)^{\beta}F_4(\tau), \tag{97}$$

$$p(r)=P(\rho), \quad K(\rho,\tau)=\frac{b-a}{2}k(r,t), \tag{98}$$

the integral equation is expressed as

$$\frac{1}{\pi}\int_{-1}^{1}\left[\frac{1}{\tau-\rho}+K(\rho,\tau)\right]F_4(\tau)(1-\tau)^{-1/2}(\tau+1)^{\beta}\,d\tau=-P(\rho), \quad -1<\rho<1. \tag{99}$$

The function $F_4(\tau)$ is obtained by using a Gauss-Jacobi-type quadrature formula (Erdogan *et al.*, 1973) and solving the singular integral eqn (99) together with the additional condition $F_4(1)=0$, to account for the boundedness of $\phi(t)$ at $t=b$.

The mode I stress intensity factor at the crack tip a is defined by

$$K(a)=\lim_{r\to a}2^{1/2}(a-r)^{-\beta}\sigma_{zz}^{0}(r,0) \tag{100}$$

and can be expressed by

$$K(a)=\mu^{*}\lim_{r\to a}2^{1/2}(r-a)^{-\beta}\phi(r)=\mu^{*}a_4^{-\beta}F_4(-1), \tag{101}$$

where $a_4=(b-a)/2$. The formula given by Krenk (1975) is used to obtain $F_4(-1)$.

RESULTS AND DISCUSSION

For each of the four different types of crack configurations considered in this paper the stress intensity factors, interfacial stresses and the stresses acting on the crack plane $z=0$ and the plane $z=h/2$ are given. Although it is not possible to present results to take into account all the different effects various material parameters have on the results, the stress intensity factors are plotted for cracks of different size for different ratios of shear moduli. The Poisson's ratios were taken as $\nu_0=\nu_1=0.25$ and $p(r)=\sigma_{zz}^{I}(r)=\sigma_0$ given by eqn (A7), the uncracked matrix stress for all the numerical examples. The stress fields are presented for a SiC/CAS calcium aluminosilicate glass ceramic reinforced with silicon carbide fibers with the following material parameters (Daniel *et al.*, 1989)

$$E_0=E_f=207\text{ GPa }(30.0\times10^6\text{ psi}), \quad E_1=E_m=98\text{ GPa }(14.2\times10^6\text{ psi})$$
$$\nu_0=\nu_f=0.25, \quad \nu_1=\nu_m=0.25, \quad V_f=0.4. \tag{102}$$

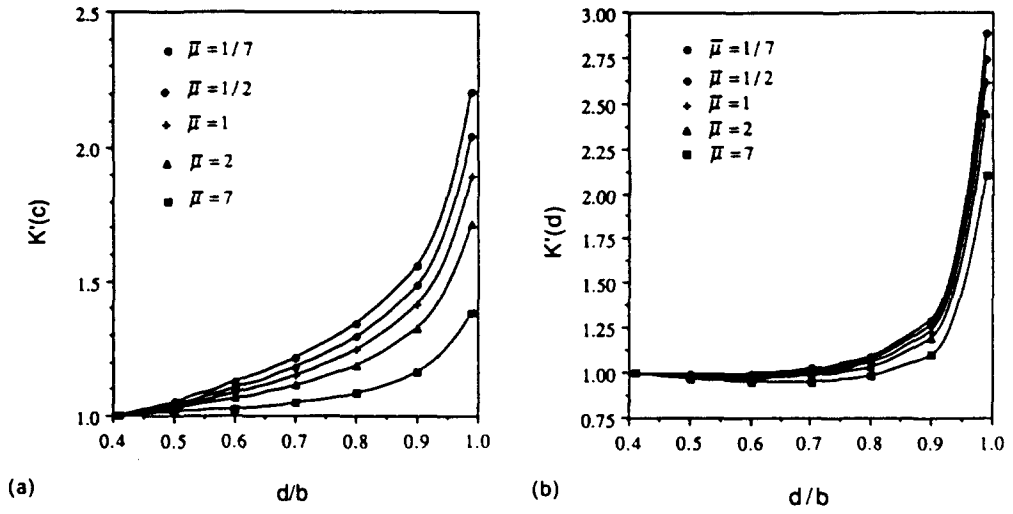

Fig. 2. Stress intensity factors for the internal annular crack with inner crack tip away from the interface (Case I), $a/h = 0.3$, $c/h = 0.4$.

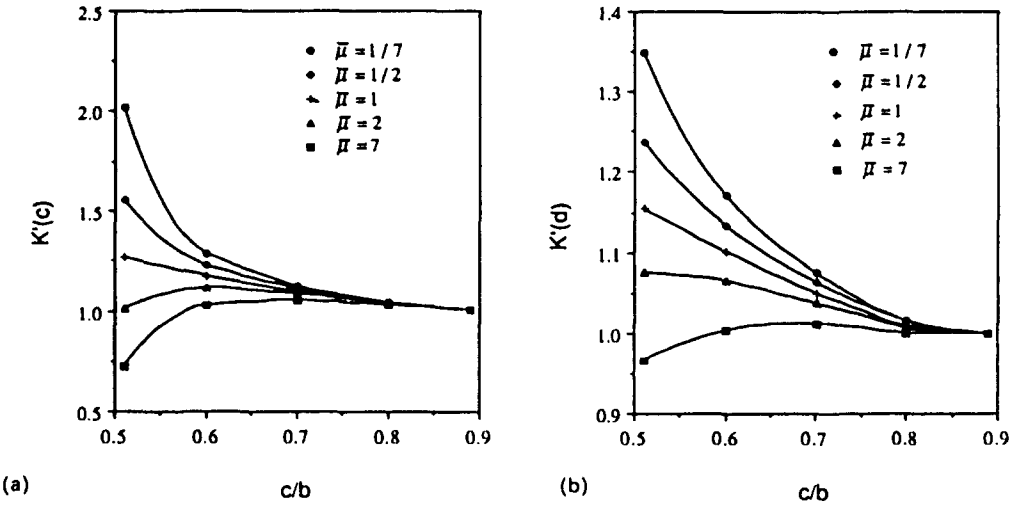

Fig. 3. Stress intensity factors for the internal annular crack with inner crack tip away from the interface (Case I), $a/h = 0.5$, $d/h = 0.9$.

For these material values $\bar{\mu} = 2.1127$ and $a/h = 0.6325$. Equations (4)–(6) and (10)–(12) are used to determine the required stresses. The results for the stresses presented are normalized with respect to the remote matrix stress σ_0, i.e. $\bar{\sigma}_{rr}(a, z) = \sigma_{rr}(a, z)/\sigma_0$ etc.

For Case I, the internal annular crack with inner crack tip away from the interface, the normalized stress intensity factors are defined by

$$K'(c) = \frac{K(c)}{\sigma_0 a_1^{\frac{1}{2}}} = F_1(-1), \quad K'(d) = \frac{K(d)}{\sigma_0 a_1^{\frac{1}{2}}} = -F_1(1). \tag{103}$$

The normalized stress intensity factors given in Fig. 2 are for the ratios $a/h = 0.3$ and $c/h = 0.4$ while in Fig. 3, $a/h = 0.5$ and $d/h = 0.9$. As expected when the crack size is very small, i.e. when $c/d \to 1.0$, $K'(c)$ and $K'(d) \to 1.0$, which is the result for the case of a Griffith crack in a homogeneous, isotropic elastic matrix in plane strain and hence the stress intensity factors are not influenced by the presence of the fiber or the curvature of the model for all

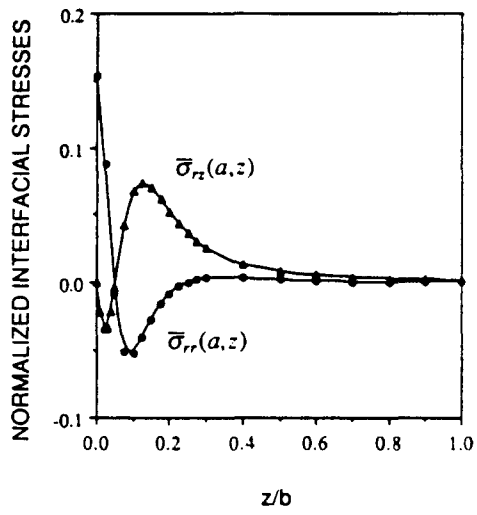

Fig. 4. Normalized interfacial stresses of the SiC/CAS composite. Case I crack configuration. $c/b = 0.7$, $d/b = 0.8$.

values of $\bar{\mu}$. For a given crack size, i.e. when d/b is held constant in Fig. 2 and c/b is held constant in Fig. 3, $K'(c)$ and $K'(d)$ decrease with increasing $\bar{\mu}$, due to the increasing stiffness of the fiber. From Fig. 3 it is also noted that when the fiber is weaker than the matrix, i.e. $\bar{\mu} < 1$, $K'(c) > K'(d)$ which indicates that the crack would propagate inward toward the center of the fiber. The effect of the stiffness of the fiber can also be observed in Fig. 3, where d/b is held fixed and $c \to a$, from the fact that when $\bar{\mu} > 1$, $K'(c) < K'(d)$ and when $\bar{\mu} < 1$, $K'(c) > K'(d)$. The stress fields for the SiC/CAS composite are given in Figs. 4–6 for the ratios $c/b = 0.7$ and $d/b = 0.8$. The interfacial radial stress $\bar{\sigma}_{rr}(a, z)$ attains a maximum value at the crack plane $z = 0$, then decreases due to the opening of the crack before reaching the remote interfacial value. The tensile radial stresses near the crack plane could lead to interfacial debonding. The interfacial shear stress $\bar{\sigma}_{rz}(a, z)$ is zero at the crack plane due to symmetry considerations and changes sign before reaching a maximum value at $\approx a/5$, the region where $\bar{\sigma}_{rr}(a, z)$ is a minimum. The axial stress distribution (Fig. 5) on the crack plane shows the singular behavior at the crack tips and the discontinuity at the interface while the stresses on the $z = h/2$ plane (Fig. 6) are nearly unperturbed by the opening of the crack.

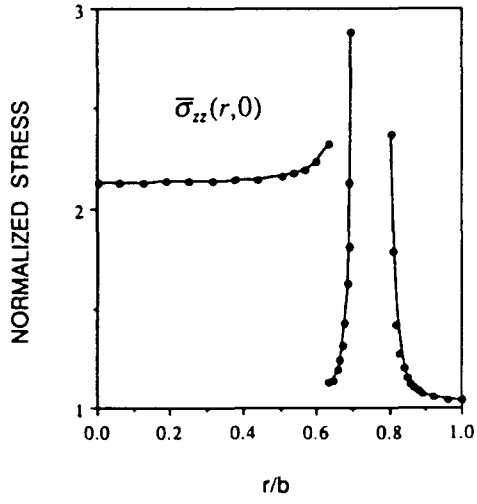

Fig. 5. Normalized axial stress on the crack plane of the SiC/CAS composite. Case I crack configuration. $c/b = 0.7$, $d/b = 0.8$.

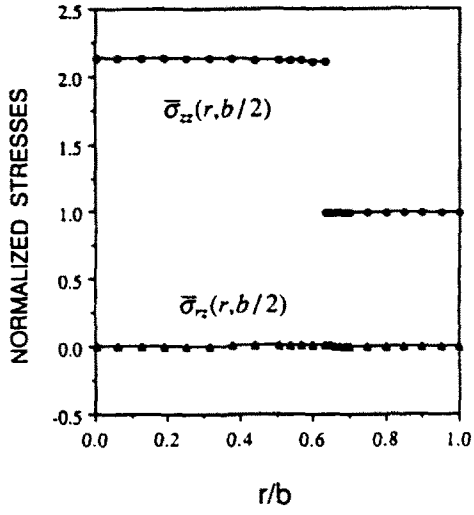

Fig. 6. Normalized stresses on the $z = b/2$ plane of the SiC/CAS composite, Case I crack configuration, $c/b = 0.7$, $d/b = 0.8$.

For the internal annular crack with inner crack tip at the interface, i.e. Case II, the normalized stress intensity factors are defined by

$$K'(a) = \frac{K(a)}{\sigma_0 a^{1/2-\beta}} = \mu^* F_2(-1), \quad K'(d) = \frac{K(d)}{\sigma_0 a^{1/2}} = -2^{\beta+1/2} F_2(1). \tag{104}$$

The crack tip d has a square-root singularity while β takes the values -0.3304, -0.4295, -0.5, -0.5755 and -0.7149 for $\bar{\mu} = 7.0$, 2.0, 1.0, 1/2 and 1/7, respectively. As expected, the singularity increases as the stiffness of the fiber decreases. Figure 7 shows the normalized stress intensity factors for $a/b = 0.5$. It is not possible to compare $K'(a)$ for different ratios of $\bar{\mu}$ since the crack tip singularity at a is dependent on $\bar{\mu}$. For a given value of $\bar{\mu}$, $K'(a)$ increases as the outer crack tip approaches the boundary. Only for $\bar{\mu} = 1.0$, when $d \to a$, $K'(a)$ and $K'(d) \to 1.0$, the reason being that $K'(a)$ and $K'(d)$ are dependent on β as indicated by eqn (104). At the outer crack tip $K'(d)$ increases with decreasing $\bar{\mu}$ since the

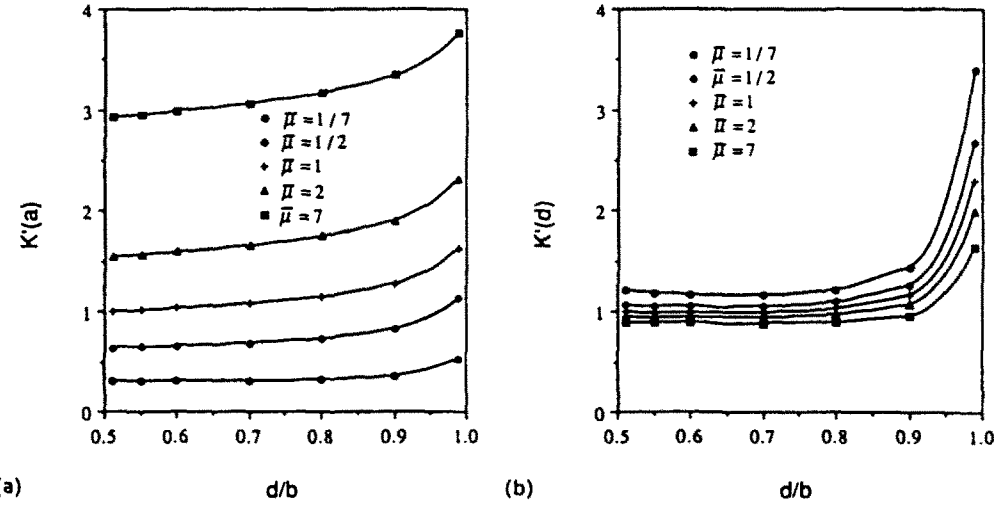

Fig. 7. Stress intensity factors for the internal annular crack with inner crack tip at the interface (Case II), $a/b = 0.5$.

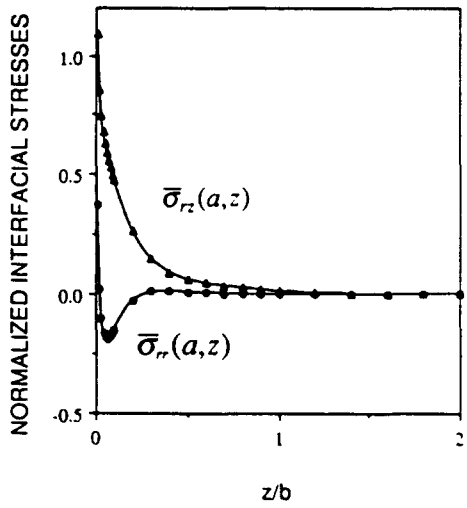

Fig. 8. Normalized interfacial stresses of the SiC/CAS composite, Case II crack configuration, $d/h = 0.9$.

outer crack tip singularity is independent of $\bar{\mu}$. Figures 8–10 show the stress fields for the SiC/CAS composite for a ratio of $d/h = 0.9$, where for the material properties given by eqn (102), $\beta = -0.4242$. The interfacial stresses are given in Fig. 8, where both stresses are singular as the crack plane is approached. The stress $\bar{\sigma}_{rr}(a, z)$ shows the effect of the crack opening up by the drop in stress prior to attaining the remote stress value, while $\bar{\sigma}_{rz}(a, z)$ decreases monotonically to zero away from the crack plane. In Fig. 9, $\bar{\sigma}_{zz}(r, 0)$ shows the expected singular behavior at the crack tips while in Fig. 10 the stresses are once again quite close to the far field stresses.

For Case III, the annular edge crack with the inner crack tip away from the interface, the normalized stress intensity factor is defined by

$$K'(c) = \frac{K(c)}{\sigma_0 a^{1/2}} = F_3(-1). \tag{105}$$

Figure 11 shows $K'(c)$ for the ratio $a/h = 0.5$. When the crack size is very small (i.e. $c/h \to 1.0$), $K'(c) \to 1.42$ and once again the stress intensity factor is not sensitive to the presence

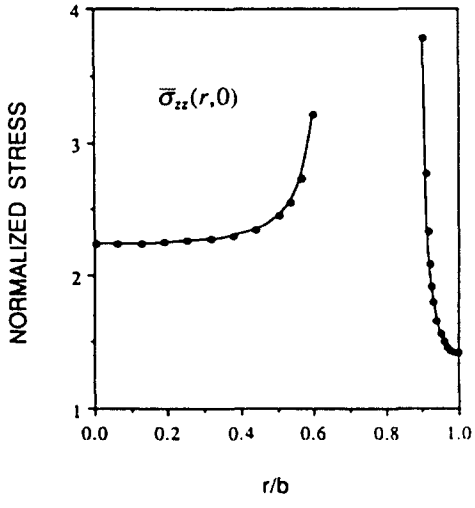

Fig. 9. Normalized axial stress on the crack plane of the SiC/CAS composite, Case II crack configuration, $d/h = 0.9$.

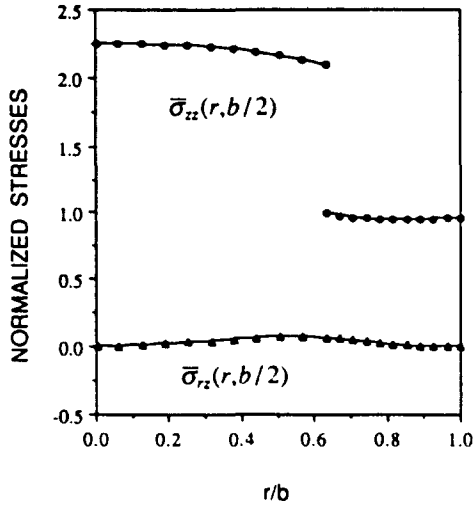

Fig. 10. Normalized stresses on the $z = b/2$ plane of the SiC/CAS composite. Case II crack configuration, $d/b = 0.9$.

of the fiber. In eqn (105) the normalizing factor contains the term $a_3^{1/2}$ where a_3 is half the crack length. If $(2a_3)^{1/2}$ instead of $a_3^{1/2}$ were used to evaluate $K'(c)$ then $K'(c) \to 1.0$ as $c/b \to 1.0$, since the two adjoining edge cracks from two adjacent cylindrical cells would then model the case of a Griffith crack in a homogeneous, isotropic elastic matrix under plane strain conditions. The stress field for the SiC/CAS composite is given in Figs 12–14 for $c/b = 0.7$. The behavior of the interfacial stresses $\bar{\sigma}_{rr}(a, z)$ and $\bar{\sigma}_{rz}(a, z)$ is similar to that shown in Fig. 4 for Case I; $\bar{\sigma}_{rr}(a, z)$ attains a maximum value at the crack plane and decreases before attaining the far-field interfacial value. The shear stress $\bar{\sigma}_{rz}(a, z)$ is zero when $z = 0$ and changes sign before reaching a maximum value at $\approx a/3$. The axial stress on the crack plane given in Fig. 13 shows the discontinuity of stress at the interface and singular behavior at the crack tip. In Fig. 14 the stresses on the plane $z = b/2$ shows the effect of the edge crack, since the remote stress field given in Appendix A shows that there is no shear stress and that the axial stresses are constant.

Finally for Case IV, the annular edge crack with inner crack tip at the interface, the normalized stress intensity factor is defined by

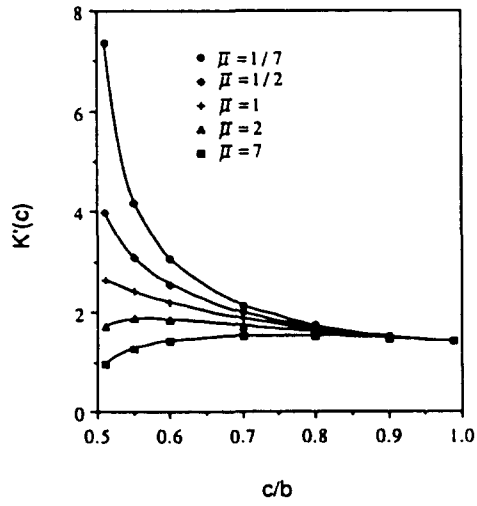

Fig. 11. Stress intensity factor for the annular edge crack with inner crack tip away from the interface (Case III), $a/b = 0.5$.

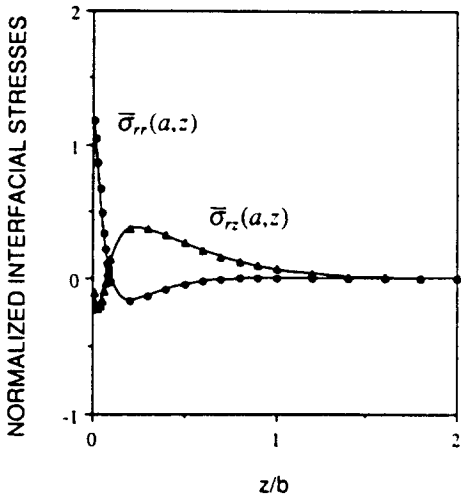

Fig. 12. Normalized interfacial stresses of the SiC/CAS composite, Case III crack configuration, $c/b = 0.7$.

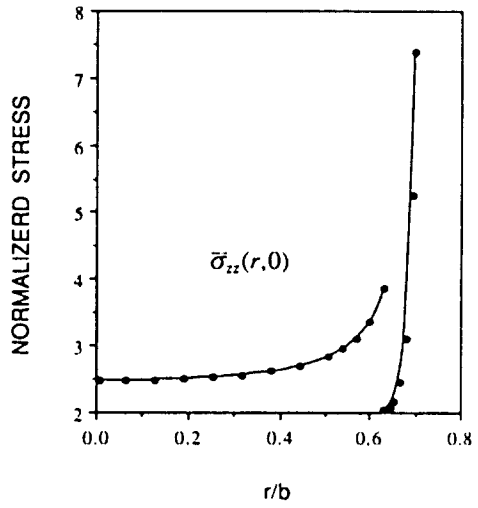

Fig. 13. Normalized axial stress on the crack plane of the SiC CAS composite, Case III crack configuration, $c/b = 0.7$.

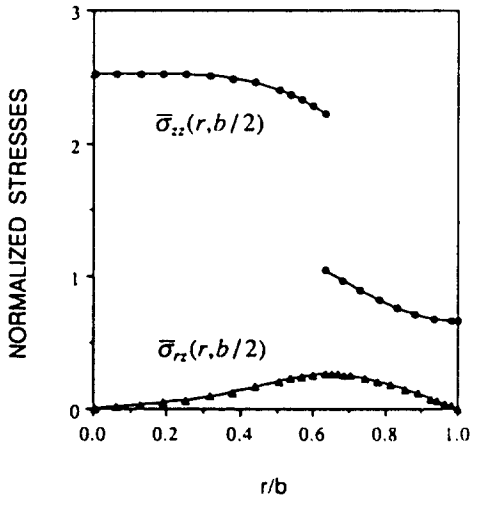

Fig. 14. Normalized stresses on the $z = h_f/2$ plane of the SiC/CAS composite, Case III crack configuration, $c/b = 0.7$.

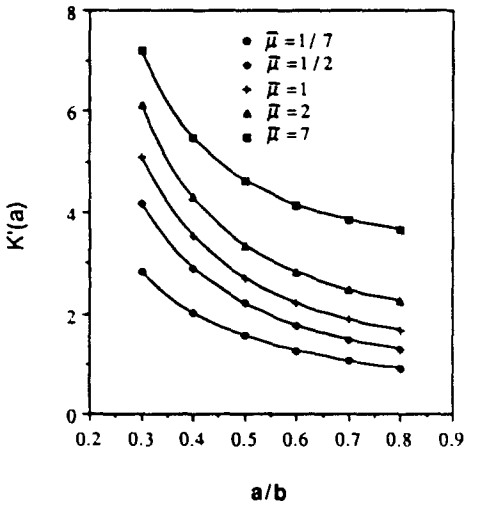

Fig. 15. Stress intensity factor for the annular edge crack with inner crack tip at the interface (Case IV).

$$K'(a) = \frac{K(a)}{\sigma_0 a_4^{\beta}} = \mu^* F_4(-1). \tag{106}$$

The normalized stress intensity factor $K'(a)$ is given in Fig. 15 and, similar to Case II, it is not possible to compare $K'(a)$ for different ratios of $\bar{\mu}$ since the crack tip singularity at a depends on $\bar{\mu}$. The interfacial stresses given in Fig. 16 have the same behavior as the interfacial stresses given in Fig. 8 for Case II. The radial stress $\bar{\sigma}_{rr}(a, z)$ attains the remote stress value at a distance approximately one fiber diameter away from the crack plane. When approaching the crack plane $\bar{\sigma}_{rr}(a, z)$ first decreases due to the presence of the crack and then exhibits singular behavior as the crack tip is approached. The shear stress $\bar{\sigma}_{rz}(a, z)$ is zero at a distance $\approx 3a$ and keeps increasing as the crack tip is neared till it becomes unbounded. Figure 17 shows the axial stress distribution in the fiber which is singular as the interface is approached. The stress field on the plane $z = b/2$ shown in Fig. 18 is perturbed from the remote stress field due to the presence of the crack.

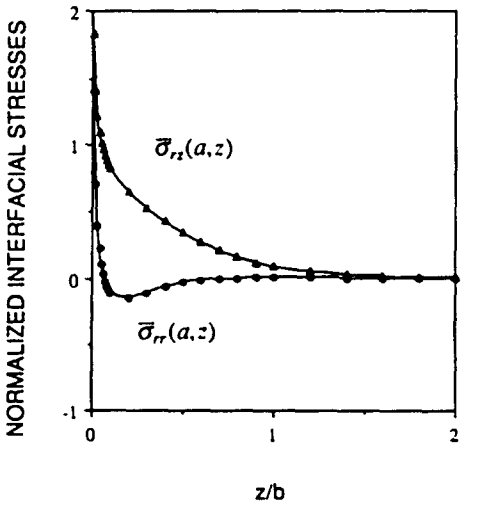

Fig. 16. Normalized interfacial stresses of the SiC/CAS composite, Case IV crack configuration.

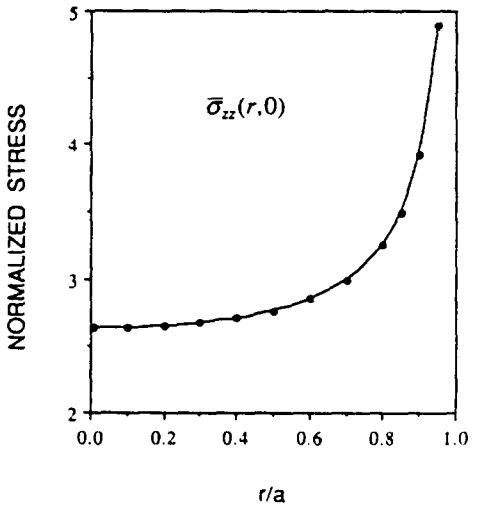

Fig. 17. Normalized axial stress on the crack plane of the SiC CAS composite, Case IV crack configuration.

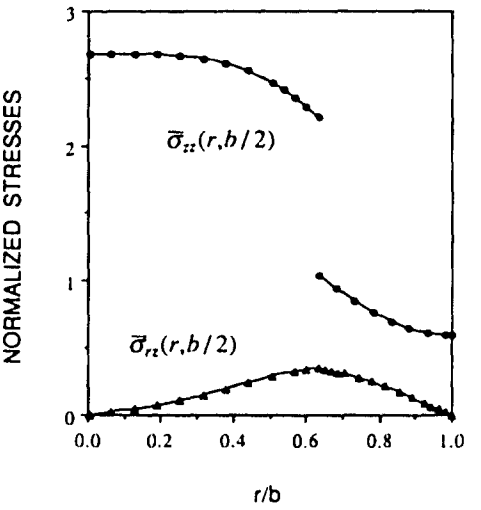

Fig. 18. Normalized stresses on the $z = b/2$ plane of the SiC/CAS composite, Case IV crack configuration.

Acknowledgements—The authors are pleased to acknowledge support from the Air Force Office of Scientific Research under Grant AFOSR-88-0124. They are grateful for helpful discussions with Professors J. D. Achenbach and I. M. Daniel during the course of this research and to Lt Col. George Haritos of the AFOSR for his encouragement and cooperation.

REFERENCES

Aveston, J., Cooper, G. A. and Kelly, A. (1971). Single and multiple fracture. In *Conf. on The Properties of Fiber Composites*, National Physical Laboratory, Guildford, Surrey, pp. 15–26. IPC, Guildford, U.K.

Aveston, J. and Kelly, A. (1973). Theory of multiple fracture of fibrous composites. *J. Mater. Sci.* **8**, 352–362.

Budiansky, B., Hutchinson, J. W. and Evans, A. G. (1986). Matrix fracture in fiber-reinforced ceramics. *J. Mech. Phys. Solids* **34**(2), 167–189.

Daniel, I. M., Anastassopoulos, G. and Lee, J.-W. (1989). Experimental micromechanics of brittle-matrix composites. In *Micromechanics: Experimental Techniques* (Edited by W. N. Sharpe Jr), AMD Vol. 102, pp. 133–146. ASME, New York.

Erdelyi, A., ed. (1954). *Tables of Integral Transforms*, Vols 1–2. McGraw-Hill, New York.

Erdogan, F. and Gupta, G. D. (1972). On the numerical solution of singular integral equations. *Q. Appl. Math.* **30**, 533–547.

Erdogan, F., Gupta, G. D. and Cook, T. S. (1973). Numerical solution of singular integral equations. In *Mechanics of Fracture* 1: *Methods of Analysis and Solutions of Crack Problems* (Edited by G. C. Sih), pp. 368–425. Noordhoff, Leyden.
Erdol, R. and Erdogan, F. (1978). A thick-walled cylinder with an axisymmetric internal or edge crack. *ASME J. Appl. Mech.* **45**, 281–286.
Gao, Y. C., Mai, Y.-W. and Cotterell, B. (1988). Fracture of fiber-reinforced materials. *ZAMP* **39**, 550–572.
Hill, R. (1964a). Theory of mechanical properties of fibre-strengthened materials: I. Elastic behaviour. *J. Mech. Phys. Solids* **12**, 199–212.
Hill, R. (1964b). Theory of mechanical properties of fibre-strengthened materials: II. Inelastic behaviour. *J. Mech. Phys. Solids* **12**, 213–218.
Jones, R. M. (1975). *Mechanics of Composite Materials*. Scripta, Washington.
Keer, L. M., Freedman, J. M. and Watts, H. A. (1977) Infinite tensile cylinder with circumferential edge crack. *Lett. Appl. Engng Sci.* **5**, 129–139.
Krenk, S. (1975). On the use of the interpolation polynomial for solutions of singular integral equations. *Q. Appl. Math.* **32**, 479–484.
Love, A. E. H. (1944). *A Treatise on the Mathematical Theory of Elasticity*. Dover, New York.
Marshall, D. B., Cox, B. N. and Evans, A. G. (1985). The mechanics of matrix cracking in brittle-matrix fiber composites. *Acta Metall.* **33**(11), 2013–2021.
Marshall, D. B. and Evans, A. G. (1985). Failure mechanisms in ceramic-fiber ceramic-matrix composites. *J. Am. Ceram. Soc.* **68**(5), 225–231.
McCartney, L. N. (1987). Mechanics of matrix cracking in brittle-matrix fiber-reinforced composites. *Proc. R. Soc. Lond.* **A409**, 329–350.
McCartney, L. N. (1989). New theoretical model of stress transfer between fiber and matrix in a uniaxially fibre-reinforced composite. *Proc. R. Soc. Lond.* **A425**, 215–244.
Nied, H. F. and Erdogan, F. (1983). The elasticity problem for a thick-walled cylinder containing a circumferential crack. *Int. J. Fracture* **22**, 277–301.
Prewo, K. M. and Brennan, J. J. (1982) Silicon carbide yarn reinforced glass matrix composites. *J. Mater. Sci.* **17**, 1201–1206.
Sigl, L. S. and Evans, A. G. (1989). Effects of residual stress and frictional sliding on cracking and pull-out in brittle matrix composites. *Mech. Mater.* **8**, 1–12.
Smith, G. E. and Spencer, A. J. M. (1970). Interfacial tractions in a fiber-reinforced elastic composite material. *J. Mech. Phys. Solids* **18**, 81–100.
Steif, P. S. (1984). Stiffness reduction due to fiber breakage. *J. Comp. Mater.* **17**, 153–172.
Timoshenko, S. P. and Goodier, J. N. (1970). *Theory of Elasticity*, 3rd edn. McGraw-Hill, New York.
Wijeyewickrema, A. C., Keer, L. M., Hirashima, K. and Mura, T. (1991) The annular crack surrounding an elastic fiber in a tension field. *Int. J. Solids Structures* **27**(3), 315–328.

APPENDIX A

Stress fields, when the fiber and matrix in the concentric cylinders model are subjected to a uniform longitudinal tensile strain ε_0 at $z = \pm\infty$ in the absence of the annular crack and the outer matrix surface is stress free, are:

$$\sigma_{rr}^0(r) = \sigma^* \tag{A1}$$

$$\sigma_{\theta\theta}^0(r) = \sigma^* \tag{A2}$$

$$\sigma_{zz}^0(r) = E_0\varepsilon_0 + 2\nu_0\sigma^* \tag{A3}$$

$$\sigma_{rz}^0(r) = 0 \tag{A4}$$

$$\sigma_{rr}^1(r) = -\sigma^*\left(\frac{a^2}{b^2-a^2}\right)\left(1-\frac{b^2}{r^2}\right) \tag{A5}$$

$$\sigma_{\theta\theta}^1(r) = -\sigma^*\left(\frac{a^2}{b^2-a^2}\right)\left(1+\frac{b^2}{r^2}\right) \tag{A6}$$

$$\sigma_{zz}^1(r) = E_1\varepsilon_0 - 2\nu_1\sigma^*\left(\frac{a^2}{b^2-a^2}\right) \tag{A7}$$

$$\sigma_{rz}^1(r) = 0 \tag{A8}$$

where

$$\sigma^* = \frac{2\varepsilon_0(\nu_0-\nu_1)V_m}{V_f/k_{p1}+V_m/k_{p0}+1/\mu_1} \tag{A9}$$

and $V_f = a^2/b^2$, $V_m = 1-V_f$, $k_{p0} = \mu_0/(1-2\nu_0)$, $k_{p1} = \mu_1/(1-2\nu_1)$ and μ, ν and E are the shear modulus, Poisson's ratio and Young's modulus, respectively. The superscripts and subscripts 0 and 1 refer to the fiber and matrix, respectively.

APPENDIX B

The functions R_{1i} $(i = 1, 3)$ and R_{2i} $(i = 2, 3)$ appearing in eqns (54) and (81), respectively, are given by

$$R_{11} = \frac{P_{11}}{Q_1}, \tag{B1}$$

$$R_{12} = \frac{1}{Q_1}\left(P_{12} - \frac{P_{11}Q_2}{Q_1}\right), \tag{B2}$$

$$R_{13} = \frac{1}{Q_1}\left[P_{13} - \frac{P_{12}Q_2}{Q_1} + P_{11}\left(-\frac{Q_3}{Q_1} + \frac{Q_2^2}{Q_1^2}\right)\right], \tag{B3}$$

$$R_{22} = \frac{P_{22}}{Q_1}, \tag{B4}$$

$$R_{23} = \frac{1}{Q_1}\left(P_{23} - \frac{P_{22}Q_2}{Q_1}\right), \tag{B5}$$

where

$$P_{11} = -4(1-\nu_1)(1-\tilde{\mu})(\tilde{\mu}+\kappa_0)(r-a)(t-a), \tag{B6}$$

$$P_{12} = -2(1-\nu_1)(1-\tilde{\mu})\{2(\tilde{\mu}+\kappa_0)(r-a) - 3(\tilde{\mu}+\kappa_0)(r+t-2a) + p_{121}[(r-a)(r+t-2a) - (r-a)^2]\}, \tag{B7}$$

$$P_{13}/(1-\nu_1) = -4\{\kappa_0 - 2\tilde{\mu}\nu_1(1-2\nu_0) + \tilde{\mu}^2[-\kappa_1 + 2\nu_1(1-2\nu_1)]\} + (1-\tilde{\mu})\{(r-a)p_{131} + (r+t-2a)p_{132} + [(r-a)(r+t-2a) - (r-a)^2]p_{133}\}, \tag{B8}$$

$$P_{22} = -2(1-\nu_1)(\tilde{\mu}+\kappa_0)(1+\tilde{\mu}\kappa_1)(2b-r-t), \tag{B9}$$

$$P_{23} = (1-\nu_1)\{(2b-r-t)p_{231} + 4(\tilde{\mu}+\kappa_0)(1+\tilde{\mu}\kappa_1)\}, \tag{B10}$$

$$p_{121} = (\tilde{\mu}+\kappa_0)\left(\frac{3}{4t} - \frac{1}{4r} - \frac{3}{2b}\right) - [5+7\tilde{\mu} - 4\nu_0(1+2\tilde{\mu})]/2a, \tag{B11}$$

$$p_{131} = -\frac{3}{2t}[(29+15\tilde{\mu})/4 - \nu_0(9+2\tilde{\mu})] + \left(\frac{6}{a} - \frac{1}{2r}\right)[(5+7\tilde{\mu})/4 - \nu_0(1+2\tilde{\mu})] + 3(\tilde{\mu}+\kappa_0)/b, \tag{B12}$$

$$p_{132} = \frac{9}{2}\left(\frac{1}{2t} - \frac{1}{b}\right)(\tilde{\mu}+\kappa_0) + [(5\tilde{\mu}-1) + 4\nu_0(1-2\tilde{\mu})]/8r + [(19-63\tilde{\mu})/8 - \nu_0(15-26\tilde{\mu})/2 - 4\nu_1(\tilde{\mu}+\kappa_0)]/a, \tag{B13}$$

$$p_{133} = \frac{3}{8}(\tilde{\mu}+\kappa_0)\left[\left(\frac{3}{t} - \frac{1}{r} + \frac{1}{b}\right)\Big/ b + \left(\frac{1}{rt} - \frac{3}{2r^2} + \frac{5}{2t^2}\right)\Big/ 2\right] - \frac{3}{4ab}[(5+7\tilde{\mu}) - 4\nu_0(1+2\tilde{\mu})] + \frac{3}{8a^2}[(7-19\tilde{\mu}) - 4\nu_0(1-4\tilde{\mu})], \tag{B14}$$

$$p_{231} = (1-\tilde{\mu}^2)(1-\kappa_0\kappa_1)/a + \left(\frac{3}{4t} - \frac{1}{4r}\right)(\tilde{\mu}+\kappa_0)(1+\tilde{\mu}\kappa_1), \tag{B15}$$

$$Q_1 = -2(1-\nu_1)(\tilde{\mu}+\kappa_0)(1+\tilde{\mu}\kappa_1), \tag{B16}$$

$$Q_2 = (1-\nu_1)\left\{(1-\tilde{\mu}^2)(1-\kappa_0\kappa_1)/a + \frac{3}{2b}(\tilde{\mu}+\kappa_0)(1+\tilde{\mu}\kappa_1)\right\}, \tag{B17}$$

$$Q_3 = (1-\nu_1)\left\{\frac{1}{a^2}(1-\tilde{\mu})\{-(1-\tilde{\mu})(5+8\nu_0\nu_1) + 2[\nu_0(5-2\tilde{\mu}) + \nu_1(2-5\tilde{\mu})]\} - \frac{3}{4ab}(1-\tilde{\mu}^2)(1-\kappa_0\kappa_1) + \frac{3}{16b^2}(\tilde{\mu}+\kappa_0)(1+\tilde{\mu}\kappa_1)\right\}. \tag{B18}$$

The functions S_{1i} $(i = 1, \ldots, 6)$ and T_{1i} $(i = 1, 3)$ required to define $I_{ij}^{*}(r, t)$ in eqn (55) are expressed as

$$S_{11} = -\frac{P_{11}Q_2}{Q_1^2}\frac{1}{(r+t-2a)^2}, \tag{B19}$$

$$S_{12} = \frac{(1-\tilde{\mu})(r-a)}{(\tilde{\mu}+\kappa_0)(1+\tilde{\mu}\kappa_1)(r+t-2a)} p_{121}, \tag{B20}$$

$$S_{13} = \frac{-(1-\tilde{\mu})(r-a)^2}{(\tilde{\mu}+\kappa_0)(1+\tilde{\mu}\kappa_1)(r+t-2a)^2} p_{121}, \tag{B21}$$

$$S_{14} = -\frac{P_{12}Q_2}{Q_1^2} \frac{1}{(r+t-2a)}, \tag{B22}$$

$$S_{15} = \frac{-(1-\tilde{\mu})(r-a)}{2(\tilde{\mu}+\kappa_0)(1+\tilde{\mu}\kappa_1)(r+t-2a)} p_{131}, \tag{B23}$$

$$S_{16} = \frac{-(1-\tilde{\mu})}{2(\tilde{\mu}+\kappa_0)(1+\tilde{\mu}\kappa_1)} p_{132}, \tag{B24}$$

$$T_{11} = \frac{P_{11}}{Q_1}\left(-\frac{Q_3}{Q_1} + \frac{Q_2^2}{Q_1^2}\right) \frac{1}{(r+t-2a)}, \tag{B25}$$

$$T_{12} = \frac{-(1-\tilde{\mu})(r-a)}{2(\tilde{\mu}+\kappa_0)(1+\tilde{\mu}\kappa_1)} p_{133}, \tag{B26}$$

$$T_{13} = \frac{(1-\tilde{\mu})(r-a)^2}{2(\tilde{\mu}+\kappa_0)(1+\tilde{\mu}\kappa_1)(r+t-2a)} p_{133}. \tag{B27}$$

The functions S_{2i}, $(i = 1, 2)$ required to define $I_2^{b,t}(r, t)$ in eqn (82) are given by

$$S_{21} = -\frac{P_{22}Q_2}{Q_1^2} \frac{1}{(2b-r-t)} \tag{B28}$$

$$S_{22} = \frac{-1}{2(\tilde{\mu}+\kappa_0)(1+\tilde{\mu}\kappa_1)} p_{231}. \tag{B29}$$